Fluorescence microscopic imaging through tissue-like turbid media

X. S. Gan and M. Gu[a)]
Optoelectronic Imaging Group, School of Communications and Informatics, Victoria University of Technology, P.O. Box 14428, MCMC, Victoria 8001, Australia

(Received 23 June 1999; accepted for publication 20 December 1999)

In this article, effective point spread functions for fluorescence microscopic imaging are introduced to investigate the effects of scattering particle size and optical gating on image resolution under single-photon ($1p$) and two-photon ($2p$) excitation. The dependence of image resolution on these effects shows a deeper penetration depth under $2p$ excitation due to the use of a longer illumination wavelength and the nonlinear dependence of the fluorescence on excitation intensity. The fundamental difference between $1p$ and $2p$ fluorescence imaging is that $1p$ fluorescence imaging mainly depends on the fluorescence light excited by scattered photons, in which case the penetration depth is limited by the degradation in image resolution. However, $2p$ fluorescence imaging is determined by the fluorescence light excited by ballistic photons, in which case the penetration depth is limited by the loss in signal strength. The results also reveal that the pinhole gating method is efficient in $1p$ fluorescence imaging, but exhibits a limited influence on $2p$ fluorescence imaging. It is also demonstrated that in $2p$ fluorescence imaging, a high numerical aperture objective gives a strong signal while retains an image of high resolution if the turbid medium is not so thick. © *2000 American Institute of Physics.* [S0021-8979(00)01407-9]

I. INTRODUCTION

Optical imaging through turbid media has been an active research area for a decade because of its potential applications in noninvasive medical imaging and diagnosis.[1,2] Fluorescence imaging, which can be achieved under single-photon $1p$ and two-photon[3] ($2p$) excitation, is one of the main tools in medical diagnosis of human diseases.[4,5] The key problem associated with fluorescence imaging through a turbid tissue medium is the strong scattering effect that severely degrades image quality. A number of gating techniques have been introduced to suppress multiply scattered photons which carry less information about an object embedded in a turbid medium. These techniques include time gating,[6–8] polarization gating,[9,10] coherence gating,[11,12] space gating,[13,14] angle gating methods,[15,16] etc.

Due to the fact that the excitation of fluorescence light demolishes or reduces coherence and polarization properties, some gating techniques may not be efficient in fluorescence imaging through turbid media. Another fact that has to be taken into account is that fluorescence excitation, particularly $2p$ fluorescence excitation,[3] requires a high concentration of power, and therefore microscope objectives are inevitably introduced to focus the illumination light into a turbid tissue sample. Although there are a number of publications on microscopic imaging through turbid media (the pinhole gating method,[14,17] the space gating method,[13,14] the angle gating methods utilizing annular lenses,[15,16,18] etc.), the investigation into fluorescence microscopic imaging is not extensive. An experiment study of fluorescence microscopic imaging through turbid media has been recently performed[19,20] and a Monte Carlo simulation model has been developed for fluorescence microscopy.[21,22] This model has been used to explain the signal reduction in a turbid medium. However, the effect of scattering on image resolution and optical gating methods has not been studied. The motivation of this article is to investigate fluorescence microscopic image formation, in particular, image resolution under $1p$ and $2p$ excitation. The method used in this article is based on the concept of the effective point spread function (EPSF).[23]

This article is organized as follows. In Sec. II, an introduction to the concept of the EPSF for fluorescence microscopic imaging through turbid media is presented. $1p$ and $2p$ fluorescence imaging is discussed Secs. III and IV, respectively. In both cases, the focus of the investigation is centered on the effect of the size of scattering particles and optical gating on image resolution. A discussion is presented in Sec. V and finally, a conclusion is given in Sec. VI.

II. EFFECTIVE POINT SPREAD FUNCTIONS IN A TURBID MEDIUM UNDER 1p AND 2p EXCITATION

A Monte Carlo simulation method has been developed for fluorescence microscopic imaging.[21,22] However, the simulation method is slow in image modeling, particularly when an embedded object has a complex structure. Here, we extend this simulation model, based on the concept of the EPSF.[23]

In our Monte Carlo simulation model similar to the reported one,[23] the spatial coordinates x, y, z, and angular coordinates θ and φ are used to trace the position and direction of each photon. A parameter p is assigned to each photon to represent its weighting in signal strength. $1p$ fluorescence excitation is a linear process in which case the excited fluorescence intensity is proportional to the incident intensity. Therefore, the weighting of an emitted fluorescence photon

a)Electronic mail: ming@dingo.vu.edu.au

is linearly proportional to the weighting of the incident photon:[21]

$$p_{1f} = \alpha_{1p} p_e , \tag{1}$$

where α_{1p} is a $1p$ fluorescence coefficient, and p_{1f} and p_e are, respectively, the weighting factors of the incident and fluorescence photons.

However, $2p$ fluorescence is a nonlinear process in which case the excited fluorescence light intensity has a quadratic response to the excitation light intensity:

$$I_{2p} = \alpha_{2p} I_{\text{ex}}^2, \tag{2}$$

where α_{2p} is a $2p$ fluorescence coefficient, and I_{2p} and I_{ex} are, respectively, the intensity of the incident and the fluorescence light. Because of the nonlinear process, the implementation of Eq. (2) in the Monte Carlo simulation model under $2p$ excitation is not as straightforward as that under $1p$ excitation. The execution of the Monte Carlo simulation for $2p$ excitation is divided into two stages. In the first stage, the intensity distribution of the excitation light at the focal plane, $I_{\text{ex}}(r)$, is calculated and stored in the database, which r is the radial coordinate. In the second stage, the simulation starts at the focal plane, fluorescence photons are generated by a uniform random generator. However, the weighting factor for a fluorescence photon at a distance r is determined according to the square of the local intensity of excitation light:[21,22]

$$p_{2p}(r) = \alpha_{2p} I_{\text{ex}}^2(r). \tag{3}$$

To simulate the image of a fluorescence object embedded in turbid media, we introduce an EPSF[23] under $1p$ and $2p$ excitation. An EPSF not only includes the imaging properties of a microscope but also the scattering properties of a turbid medium in which a fluorescence object is embedded. The EPSF is derived from the product of the probability of an excitation photon reaching the focal plane and the probability of a fluorescence photon reaching the detector and the detail of the derivation has been reported elsewhere.[23] The significance of an EPSF is that it enables us to separate the information of an object from a surrounding turbid medium and an imaging system. With a derived EPSF, the image intensity $I(x,y)$ of a thin object can be modeled by the convolution of an object function $O(x,y)$ and the EPSF $h(x,y)$:

$$I(x,y) = \int \int_{-\infty}^{\infty} h(x,y) O(x-x', y-y') dx' dy', \tag{4}$$

where $h(x,y)$ is the EPSF in the focal plane under $1p$ and $2p$ excitation. 10 000 000 illumination photons are used in the Monte Carlo simulation to ensure the accuracy of an EPSF for a reflection-mode scanning optical microscope shown in Fig. 1. $L_1$and L_2 are two identical objectives used for illumination and detection, respectively. A finite-sized pinhole of diameter ν_d is placed in front of the detector.

It is assumed that under $1p$ excitation the wavelength of the excitation beam and fluorescence beam is 400 nm, whereas under $2p$ excitation, the excitation and fluorescence wavelengths are 800 and 400 nm, respectively. The scattering medium consists of either spherical particles of diameter (ρ) 0.48 μm or spherical particles of diameter 0.202 μm,

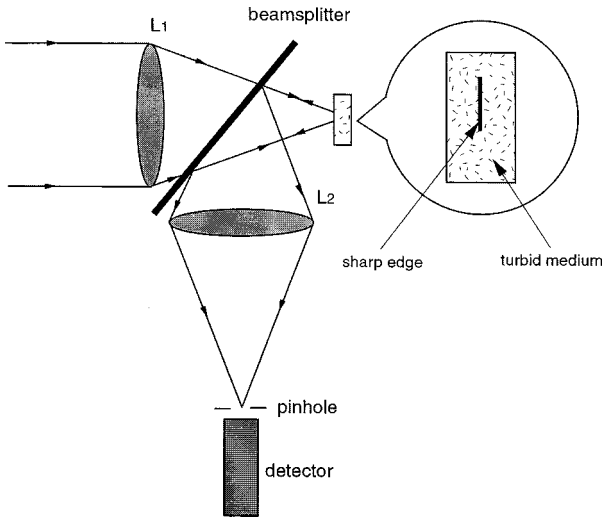

FIG. 1. Schematic diagram of a reflection-mode scanning optical microscope.

suspended in water. We assume that the particle concentration in the turbid medium consisting of 0.48 μm particles is $0.87\times10^9/\text{mm}^3$. According to Mie Scattering theory,[24] the corresponding scattering mean-free path length (SMFPL) l is 3.68 and 15 μm, respectively for wavelengths 400 and 800 nm. The optical thickness n is defined as the sample thickness d divided by the SMFPL l. For example, if a sample is embedded at a depth of 30 μm, the corresponding optical thickness is 8.14 for wavelength 400 nm. In order to demonstrate the effect of particle size, the SMFPL in a turbid medium consisting of 0.202 μm particles is also assumed to be 3.68 and 15 μm, respectively, for wavelengths 400 and 800 nm. The parameters associated with the two turbid media are summarized in Table I. On the basis of the concept of the EPSF and Eq. (4), the effects of the size of scattering particles and optical gating on $1p$ and $2p$ fluorescence imaging through turbid media are investigated in the following sections.

III. SINGLE-PHOTON FLUORESCENCE IMAGING THROUGH TURBID MEDIA

A. Influence of the size of scattering particles

The EPSF for $1p$ fluorescence imaging at different focal depths is shown in Fig. 2. It is noticed that the EPSF becomes broader with increasing the depth. For example, the full width at half maximum (FWHM) of the EPSF increases by 96% and 215%, respectively, at depths of 22.5 and 30 μm, compared with the FWHM of the EPSF at $d=15$ μm. The result shown in Fig. 2 demonstrates that the scattering effect in a turbid medium can severely degrade image reso-

TABLE I. Parameters associated with scattering media.

	$\lambda=400$ nm		$\lambda=800$ nm	
ρ(μm)	g	SMFPL (μm)	g	SMFPL (μm)
0.48	0.89	3.68	0.73	15
0.202	0.69	3.68	0.2	15

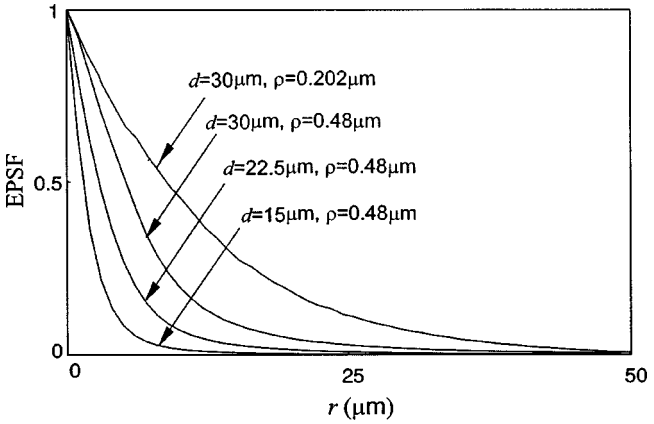

FIG. 2. EPSF for $1p$ fluorescence imaging at different depths d for scatterers of diameters 0.48 and 0.202 μm, respectively ($\nu_d \to \infty$, NA=0.25).

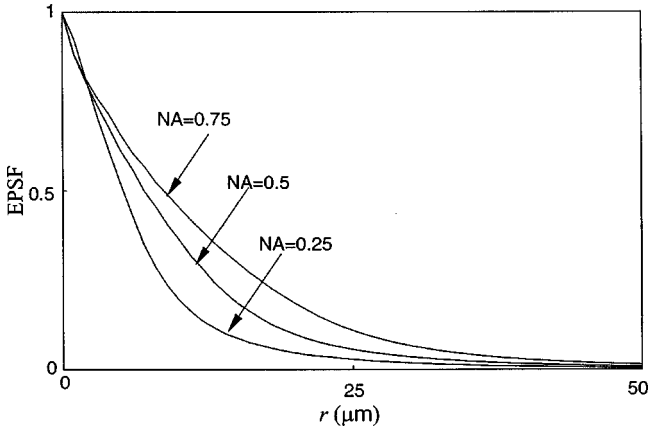

FIG. 4. EPSF at a depth of 30 μm for different values of the numerical aperture of an objective in $1p$ fluorescence imaging ($\nu_d \to \infty$, $\rho = 0.48$ μm).

lution, because scattered photons deviate from the paths of ballistic photons and form a broad distribution in the focal plane. The more scattering events a photon experiences, the larger the deviation it produces, which results in a broader EPSF.

The EPSF at a depth of 30 μm in a turbid medium consisting of 0.202 μm particles is also included in Fig. 2 for comparison. It is demonstrated that the EPSF is broader for a turbid medium consisting of small scattering particles. This feature is due to the fact that the anisotropy value g is smaller for smaller scatterers (see Table I). Therefore, a scattered photon statistically deviate further from the paths of ballistic photons after each scattering event, which leads to a broader EPSF.

To characterize image resolution, we consider a thin sharp edge embedded in a scattering slab. From the image intensity of the sharp edge scanned in the x direction, the transverse resolution, Γ, is defined as the distance between the 90% and 10% intensity points.

Transverse image resolution of an edge object embedded in a turbid medium consisting of either particles of diameter 0.48 μm or particles of diameter 0.202 μm is illustrated in Fig. 3. It is shown that the transverse resolution degrades when a turbid medium becomes thick and that the resolution becomes worse if a turbid medium consists of smaller scatterers as the result of a broader EPSF shown in Fig. 2.

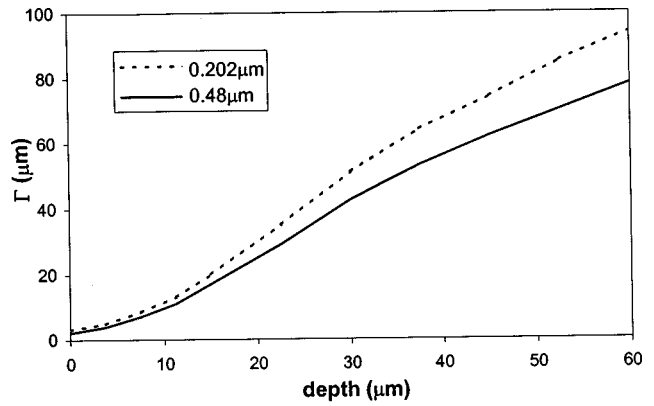

FIG. 3. Transverse resolution of a thin edge image as a function of the focal depth for different sizes of scattering particles in $1p$ fluorescence imaging ($\nu_d \to \infty$, NA=0.25).

B. Effect of optical gating

One way to improve image quality in imaging through a turbid medium is to suppress the contribution of highly scattered photons by using optical gating methods. One of the most efficient optical gating methods used in microscopic imaging is the pinhole gating method.[14,17] Before a pinhole mask starts to play its role, photons emerging from a turbid medium go through a preselection process determined by the aperture of objectives. In this section, we will demonstrate the influence of the numerical aperture of objectives and size of confocal pinholes on $1p$ fluorescence imaging through a turbid medium.

The EPSF at a depth of 30 μm for $1p$ fluorescence imaging is shown in Fig. 4 for different values of the numerical aperture of an objective. It is found that a narrow central peak becomes visible at the focal center for high numerical aperture objectives (NA=0.5 and 0.75). The central peak is mainly contributed by ballistic photons which suffer no scattering effect on their way propagating to the focal center. These ballistic photons form a diffraction-limited spot. For high numerical aperture objectives, the focal spot is small, which leads to a high intensity at the focal center. However, the other components in the EPSF, contributed by scattered photons, form a broad distribution for high numerical aperture objectives. This is because a high numerical aperture objective collects scattered photons travels at high angles and these scattered photons statistically experience more scattering events and contribute to a broader distribution in the EPSF.

In Fig. 5, transverse resolution as a function of the optical thickness is illustrated for different values of the numerical aperture of an objective. It is shown that for a higher numerical aperture objective, the transverse resolution is poorer at a given focal depth if $d > 5$ μm. This is because the scattered components in the EPSF are dominant in forming an image. In this case, more scattered photons are collected by the objective, and the corresponding distribution in

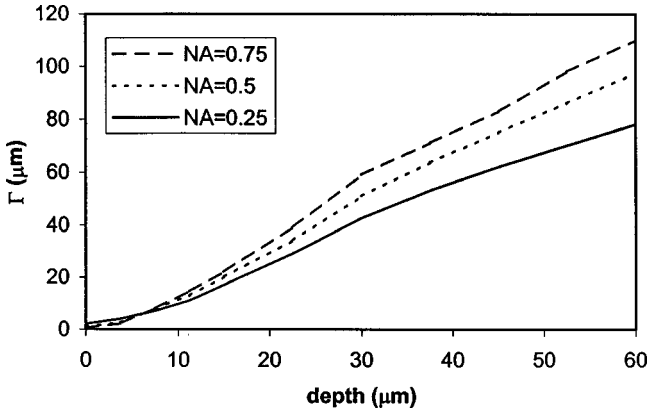

FIG. 5. Transverse resolution for different values of the numerical aperture of an objective in $1p$ fluorescence imaging ($\nu_d \to \infty$, $\rho = 0.48$ μm).

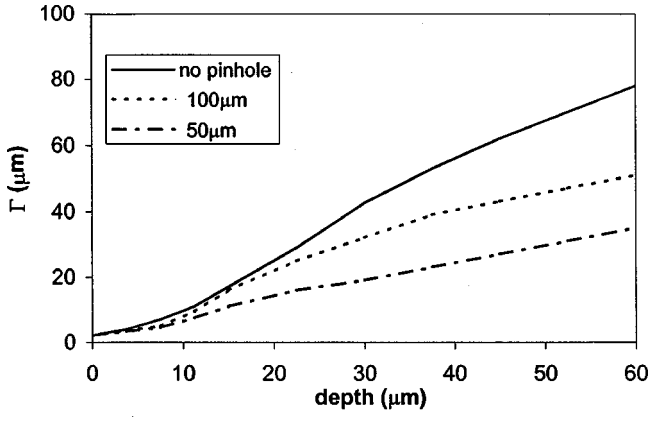

FIG. 7. Transverse resolution for different sizes of a pinhole in $1p$ fluorescence imaging (NA=0.25, $\rho = 0.48$ μm).

the EPSF is broad (see Fig. 4), which leads to a poorer transverse resolution. However a higher numerical aperture objective also gives a sharper distribution in the EPSF for ballistic component (see Fig. 4), which gives a better resolution, when $d < 5$ μm. But the strength of such component is weaker compared with scattered component for a thicker turbid medium. As the result, using a higher numerical aperture objective without other gating methods, such as pinhole gating[14,17] in $1p$ fluorescence imaging, gives a poorer transverse resolution.

To demonstrate the effect of pinhole gating on fluorescence microscopic imaging, we show the EPSF at a depth of 30 μm for different sizes of pinhole in Fig. 6. It is noted that with the utilization of a confocal pinhole, the EPSF becomes slightly narrower; the smaller the size of the pinhole, the narrower the EPSF. It is also noticed that the tail of the EPSF drops quickly when a pinhole is used. This feature shows that pinhole gating is particularly efficient in suppressing highly scattered photons which deviate further from the path of ballistic photons. The elimination of the long tail may significantly reduce the blurring of an image caused by the scattering effect. In Fig. 7, the transverse resolution as a function of the focal depth is illustrated for different sizes of pinhole. As expected, the transverse resolution improves significantly when a pinhole is used. For example, at a depth of 45 μm, the transverse resolution is 62.2 μm when no confocal pinhole is used, but becomes 42.8 and 27.1 μm, respectively, for a pinhole of diameters 100 and 50 μm. The ratio of improvement is 31.2% and 56.4% in these two cases, respectively.

IV. TWO-PHOTON FLUORESCENCE IMAGING THROUGH TURBID MEDIA

A. Effect of the size of scattering particles

The EPSF for $2p$ fluorescence imaging is shown in Fig. 8. It is seen that a peak is shown near the focal center. With the increase of the focal depth, the peak becomes less significant and may eventually disappear if the scattering medium is thick enough. The peak is contributed by the fluorescence light excited by ballistic photons that experience no scattering event on their way to the focal plane. The total number of these ballistic photons may be insignificant compared with scattered photons; however, their contribution to the intensity near focal region may still be significant, since these ballistic photons are only distributed near the focal region. Their contribution to the intensity is enhanced due to the quadratic intensity dependence under $2p$ excitation. If a

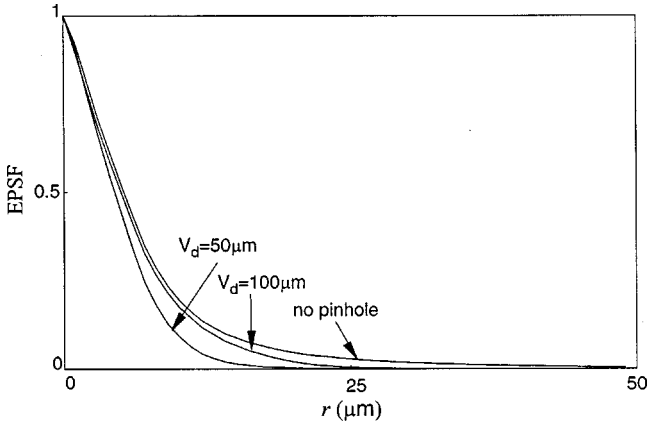

FIG. 6. EPSF at a depth of 120 μm for different sizes of a pinhole in $1p$ fluorescence imaging (NA=0.25, $\rho = 0.48$ μm).

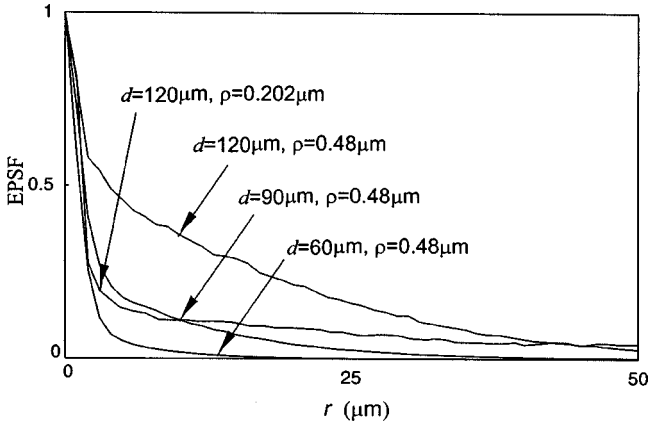

FIG. 8. EPSF for $2p$ fluorescence imaging at different depths d for scatterers of diameters 0.48 μm and 0.202 μm, respectively, ($\nu_d \to \infty$, NA=0.25).

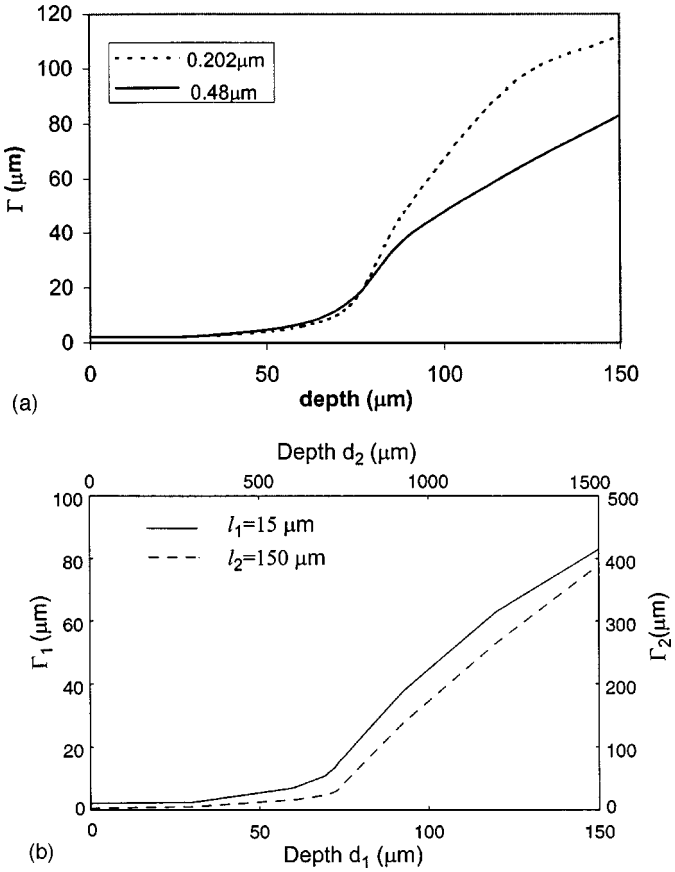

FIG. 9. (a) Transverse resolution of a thin edge image as a function of the focal depth for different sizes of scattering particles in $2p$ fluorescence imaging ($v_d \to \infty$, NA=0.25). (b) Transverse resolution Γ_1 and Γ_2 as a function of the focal depth d_1 and d_2, respectively, for SMFPLs l_1 and l_2 ($v_d \to \infty$, NA=0.25).

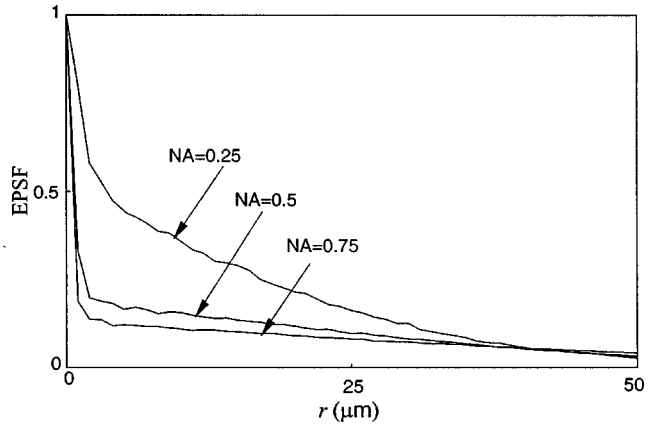

FIG. 10. EPSF at a depth of 120 μm for different values of the numerical aperture of an objective in $2p$ fluorescence imaging ($v_d \to \infty$, $\rho = 0.48$ μm).

photon experiences some scattering events, it deviates from the path of ballistic photon and forms a broad distribution on the focal plane.

The EPSF at a depth of 120 μm in a turbid medium consisting of 0.202 μm particles is also illustrated in Fig. 8. The EPSF has a stronger central peak, but is more widely distributed in this case, compared with the EPSF at the same depth in a turbid medium consisting of 0.48 μm particles. It is understood that the anisotropy value g is less for smaller scattering particles, which results in a broader distribution in the EPSF. As a result of this property, the intensity outside the focal region is relatively low in a turbid medium consisting of small scattering particles. Therefore, the central peak becomes more significant due to the quadratic intensity response under $2p$ excitation.

The transverse resolution of an edge object embedded in a turbid medium consisting of either 0.48 μm particles or 0.202 μm particles is illustrated in Fig. 9(a). A comparison of Figs. 3 and 9(a) demonstrates that $2p$ fluorescence imaging is vastly superior to $1p$ fluorescence imaging in terms of image resolution if the depth is less than 60 μm. For $2p$ fluorescence imaging, the transverse resolution stays nearly at the diffraction-limited resolution when $d<60$ μm, and then quickly increases. The increasing rate eventually drops approximately after $d=90$ μm. When $d<60$ μm, the fluorescence light excited by ballistic light is dominant over that excited by scattered light, and therefore a near diffraction-limited image resolution can be achieved. In the range of 60 μm$<d<$90 μm, the weighting of the fluorescence light excited by ballistic photons drops quickly and the fluorescence light excited by scattered photons becomes strong, thus leading to a poor transverse resolution. In this region, the increasing rate of transverse resolution depends on the decaying rate of ballistic photons. When $d>90$ μm, the scattered component in the EPSF is dominant in building an image. In this situation, the transverse resolution is decided by the broadness of the EPSF contributed by scattered photons.

A comparison of the two image resolution curves in Fig. 9(a) shows that the transverse resolution in a turbid medium consisting of 0.48 μm particles is better only when $d>75$ μm, in which case scattered photons dominate the imaging process. In the region $d<75$ μm, where the central peak in the EPSF dominates the image formation, the resolution is almost same for the two turbid media. Transverse resolution as a function of depth for different SMFPLs l_1 and l_2 is shown in Fig. 9(b). It should be pointed out that although the depth scales d_1 and d_2 have one order of magnitude difference, the optical thickness n is the same for both scales. It is shown that the transverse resolution is very close for the two media in the ballistic photon dominated regime. However, the transverse resolution is much poorer for a turbid medium of larger SMFPL l_2.

B. Effect of optical gating

In the previous section, we have demonstrated that the role of the central peak in the EPSF plays an important role in $2p$ fluorescence imaging. In this section, we will demonstrate how it can affect the optical gating efficiency in $2p$ fluorescence imaging.

The EPSF at a depth of 120 μm for $2p$ fluorescence imaging is shown in Fig. 10 for different values of the numerical aperture of an objective. The EPSF for $2p$ excitation is not necessary poorer if a higher numerical aperture objective is used. In fact, in this situation, the central peak is more pronounced, but the EPSF appears to be broader.

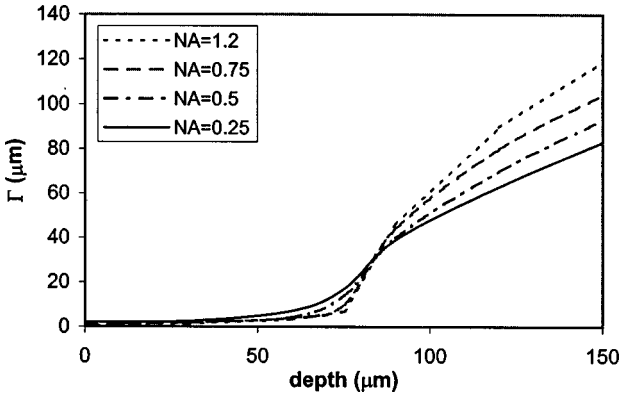

FIG. 11. Transverse resolution for different values of the numerical aperture of an objective in $2p$ fluorescence imaging ($\nu_d \to \infty$, $\rho = 0.48$ μm).

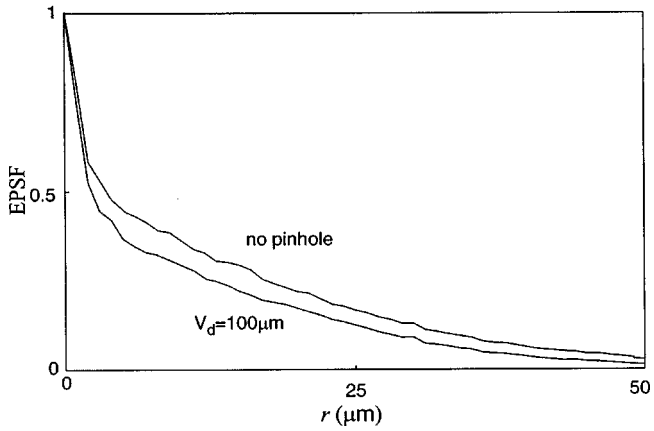

FIG. 12. EPSF at a depth of 120 μm for different sizes of a pinhole in $2p$ fluorescence imaging (NA=0.25, $\rho = 0.48$ μm).

In Fig. 11, the transverse resolution as a function of the focal depth is illustrated for different values of the numerical aperture of an objective. It is noted that for $d < 60$ μm, the image resolution is slightly better if a higher numerical aperture objective is used. In this region, the central peak in the EPSF is dominant in forming an image. The central peak in the EPSF is mainly contributed by fluorescence excited by ballistic photons. Therefore, a near diffraction-limited resolution can be achieved in this situation. Since a higher numerical aperture objective produces a narrower diffraction spot, the corresponding transverse resolution is better. In the region where $d > 90$ μm, the transverse resolution is better when a lower numerical aperture objective is used. In this region, the broad distribution in the EPSF, contributed by scattered photons, is dominant in image formation. In this situation, a high numerical aperture objective collects more scattered photons, which results in a broader distribution in the EPSF, and therefore leads to a poorer resolution. It is in the region of 60 μm$< d <$90 μm where the central peak in the EPSF starts to lose its dominance, that a quicker degradation in image resolution occurs for a higher numerical aperture objective. In conclusion, when the ballistic peak in the EPSF is dominant in forming an image, a higher numerical aperture objective offers a better resolution. When the broad distribution contributed by scattered photons is dominant, a lower numerical aperture objective gives better transverse resolution.

Now we consider the effect of a pinhole on $2p$ fluorescence imaging. The EPSF for a pinhole of diameter 100 μm at a depth of 120 μm is illustrated in Fig. 12. It is noted that the utilization of a finite sized pinhole makes little difference in the central peak of the EPSF. However, it does reduce the contribution of scattered photons in the region outside the focal center. This feature implies that a pinhole may not be efficient in improving image quality in $2p$ fluorescence imaging through turbid media if the central peak is dominant in the EPSF. In Fig. 13, the transverse resolution as a function of the focal depth is illustrated. As expected, the resolution improvement by utilization of a finite sized pinhole is not significant until a turbid medium becomes thicker, $d > 75$ μm, in which case the fluorescence excited by scattered photons is dominant.

V. DISCUSSION

In the last two sections, we have quantitatively demonstrated that $2p$ fluorescence imaging is vastly superior to $1p$ fluorescence imaging in terms of image resolution. This feature is consistent with experiment results[25] and results from the two mechanisms; the significant reduction of scattering due to the utilization of a long wavelength illumination, and the quadratic intensity dependence in $2p$ excitation. In order to have a further understanding of the comparison of image resolution between $1p$ and $2p$ fluorescence imaging, we introduce a coefficient δ, which is defined as the ratio between the power of the central peak and the total power of the EPSF. In Fig. 14, δ as a function of the focal depth is illustrated. It is noticed that δ quickly drops to zero in the case of $1p$ fluorescence imaging, which means that the central peak quickly loses its dominance in forming an image. However in the $2p$ fluorescence situation, δ first remains approximately unchanged until $d = 45$ μm or higher, which means that a near diffraction-limited resolution can be expected in this situation. The significant difference between $1p$ and $2p$ excitation situations can be explained by the following two factors. First, the excitation wavelength for $2p$ fluorescence imaging is much longer than that of $1p$ fluorescence imaging. Therefore, under $2p$ excitation, the number of the scat-

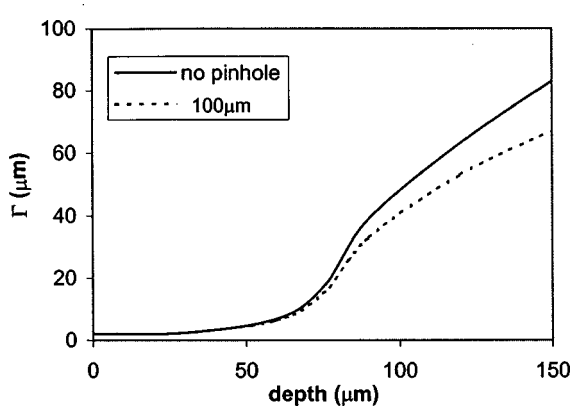

FIG. 13. Transverse resolution for different sizes of a pinhole in $2p$ fluorescence imaging (NA=0.25, $\rho = 0.48$ μm).

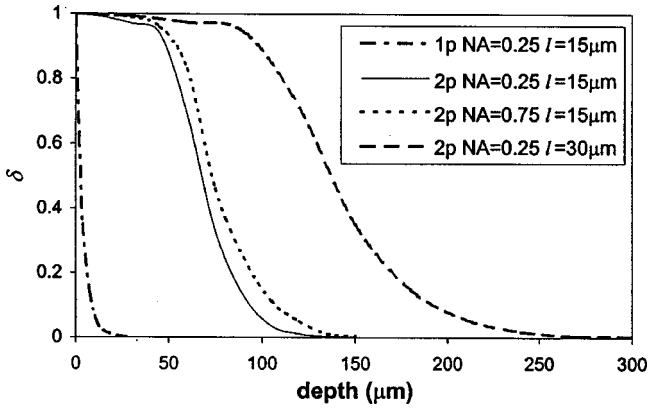

FIG. 14. δ as a function of the focal depth for $1p$ and $2p$ fluorescence imaging ($\nu_d \to \infty$, $\rho = 0.48$ μm).

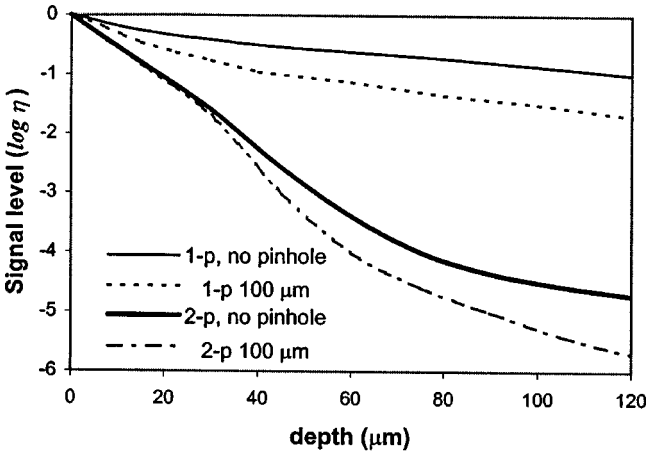

FIG. 15. Signal level as a function of the focal depth for $1p$ and $2p$ fluorescence imaging (NA$=0.25$, $\rho = 0.48$ μm).

tering events that the excitation light experiences is much less than that for $1p$ excitation. The second factor is that $2p$ excitation is a nonlinear process, which enhances the excitation near the focal center to produce a sharp peak in the EPSF. This feature shows that $1p$ fluorescence imaging is mainly determined by the fluorescence light excited by scattered photons. Thus, the degradation in image resolution limits its capacity in imaging an object deeply embedded in a turbid medium. The transition point, e.g,. $\delta = 0.5$, between ballistic photon dominated regime and scattered photon dominated regime is crucial in determining imaging performance in $2p$ fluorescence imaging. The transition point depends on parameters of a turbid medium and an imaging system. The transition point may slightly extend to deeper depth if a high numerical aperture objective, e.g., when NA $=0.75$, is used. If the SMFPL is doubled, the depth where the transition point occurs is almost doubled as well.

Here a question may be raised; what is the limit for $2p$ fluorescence imaging through a turbid medium. To answer this question, we introduce the concept of signal level η defined as the number of fluorescence photons collected by the detector. The signal level is normalized by the fluorescence signal strength when no scattering particle exists. The signal level as a function of the focal depth for $1p$ and $2p$ fluorescence imaging is shown in Fig. 15. It is noticed that the signal level in $1p$ fluorescence imaging does not decrease significantly as the turbid medium becomes thick. For example, when depth d increases to 30 μm, the image resolution drops to 42 μm (Fig. 3), while the corresponding signal level drops only to 38% (Fig. 15). However, for $2p$ fluorescence imaging, the situation is quite different. It is shown in Fig. 15 that the signal level under $2p$ excitation drops significantly when the focal depth increases. For example, the signal level drops to only 3% at $d = 30$ μm. Compared with the signal level for $1p$ fluorescence imaging, the signal level for $2p$ fluorescence imaging decreases much faster. It is also noticed that the signal level under $2p$ excitation is more than three orders of magnitude smaller than that under $1p$ excitation when $d = 60$ μm. In this situation, the $2p$ fluorescence signal may be too weak to overcome a noise level from an imaging system. However, according to Fig. 14, the $2p$ fluorescence light excited by ballistic photons is still dominant and a near diffraction-limited resolution can still be obtained at $d = 60$ μm. Therefore, we may draw a conclusion that $2p$ fluorescence imaging is mainly determined by ballistic photons, and that the penetration depth is limited by the signal level.

The image simulation of an edge object embedded in a turbid medium suggests that using a high numerical aperture objective reduces image resolution in $1p$ fluorescence imaging, since scattered photons are dominant in image formation (Fig. 4). However, in $2p$ fluorescence imaging, the utilization of a high numerical aperture objective increases signal strength without affecting image resolution in the region where the fluorescence light excited by ballistic photons in the EPSF is dominant, e.g., where $d < 60$ μm (Fig. 11). For example, at a depth of 60 μm, the signal strength for an objective of numerical apertures 0.5, 0.75, and 1.2 is, respectively, 135%, 312%, and 974% stronger than that for an objective of numerical aperture 0.25.

Using a pinhole as a spatial gating method is proven to be efficient in $1p$ fluorescence imaging through turbid media. Another issue involved in using a finite sized pinhole is that signal strength may drop significantly. According to our simulation results, at $d = 30$ μm, the signal strength for a pinhole of diameters 100 and 50 μm drops to 50% and 19% of the signal level for the no pinhole case, respectively. Since the ratio of improvement in image resolution is 31.2% and 56.4% respectively for a pinhole of diameters 100 and 50 μm in this situation, using pinhole gating in $1p$ fluorescence imaging is worthwhile. If a small pinhole is used, the loss of signal strength may cause a difficulty in detection. For example, if a pinhole of diameter 5 μm is used, the signal strength drops to less than 1%, and in this situation, the signal may be too weak to overcome the noise level for a given detector.

The utilization of a pinhole offers little improvement in $2p$ fluorescence imaging in terms of image resolution (Fig. 13). Moreover, using a pinhole significantly reduces signal strength (Fig. 15), which can be a serious problem in $2p$ fluorescence imaging through turbid media. For example, at $d = 60$ μm, the improvement in transverse resolution is only

9.5% when a pinhole of diameter 100 μm is used. However, the signal strength drops to only 31% of the signal level when no pinhole is used. It appears that using a pinhole in $2p$ fluorescence imaging through turbid media is unwise.

The simulated EPSF is contributed by two components, the narrow central peak and a broader distribution contributed by scattered photons. The central peak plays an important role in image formation under $2p$ excitation. It offers an efficient gating mechanism through the nonlinear process of $2p$ excitation. In a practical situation, the central peak in the excitation intensity distribution can be distorted by spherical aberration caused by the mismatch of refractive indices at the interface of a sample. The distortion may severely degrade image quality in $2p$ fluorescence imaging in aspects of resolution and signal strength. Therefore, it should be carefully compensated to avoid this problem.[26] In $1p$ fluorescence imaging, spherical aberration may not be a serious problem because multiple scattering in this situation plays a more pronounced role in distorting an image.

The detailed study of a two-dimensional (2D) EPSF under a fluorescence microscope provides thorough understanding of image formation through a turbid medium, which allows us to further improve image quality through mathematical reconstruction methods. The multiple scattering effect in a turbid medium also contributes to sever degradation in axial image resolution.[17,21,22] This effect can also be included in the concept of the EPSF and a 2D EPSF can be extends to a 3-D EPSF, which provides a basis for 3D image reconstruction. The detailed study of a 3D EPSF and image reconstruction based on a deconvolution algorithm will be conducted in our forthcoming publication.

VI. CONCLUSION

In conclusion, the application of the EPSF and the convolution algorithm provides us a fast and efficient image modeling method for imaging through turbid media under $1p$ and $2p$ excitation. $2p$ fluorescence imaging is generally superior to $1p$ fluorescence imaging in terms of image resolution. In the case of $2p$ fluorescence imaging, fluorescence excitation by ballistic photons dominates image formation and the penetration depth is limited because of the fast degradation in signal strength. However, for $1p$ imaging, fluorescence excitation by scattered photons is dominant, and the penetration depth is limited by the fast degradation in image resolution.

ACKNOWLEDGMENTS

The authors thank the Australian Research Council for its support.

[1] J. G. Fujimoto, S. De Silvestri, E. P. Ippen, C. A. Puliafito, R. Margolis, and A. Oseroff, Opt. Lett. **3**, 150 (1986).
[2] S. L. Jacques, Appl. Opt. **28**, 2223 (1989).
[3] W. Denk, J. H. Strickler, and W. W. Webb, Science **248**, 73 (1990).
[4] P. S. Anderson, S. Montan, and S. Svanberg, IEEE J. Quantum Electron. **QE23**, 1798 (1987).
[5] P. C. Foreman, Arch. Oral Biol. **25**, 641 (1980).
[6] K. M. Yoo and R. R. Alfano, Opt. Lett. **15**, 320 (1990).
[7] S. Anderson-Engels, R. Berg, O. Jarlmann, and S. Svanberg, Opt. Lett. **15**, 1179 (1990).
[8] D. G. Papaioannou, G. W. Hooft, J. J. M. Baselman, and M. J. C. van Gemert, Appl. Opt. **34**, 6144 (1995).
[9] F. C. Mackintosh, J. X. Zhu, D. J. Pine, and D. A. Weitz, Phys. Rev. B **40**, 9342 (1989).
[10] A. H. Hielscher, J. R. Mourant, and I. J. Bigio, Appl. Opt. **36**, 125 (1997).
[11] D. Huang, E. A. Swanson, C. P. Lin, J. S. Schuman, W. G. Stinson, W. Chang, M. R. Hee, T. Flott, K. Gregory, C. A. Pulianfito, and J. G. Fujimoto, Science **254**, 1178 (1991).
[12] M. Toida, M. Kondo, T. Ichimura, and H. Inaba, Appl. Opt. **52**, 391 (1991).
[13] M. Kempe, A. Z. Genack, W. Rudolph, and P. Dorn, J. Opt. Soc. Am. A **14**, 216 (1997).
[14] X. Gan, S. P. Schilders, and M. Gu, J. Opt. Soc. Am. A **15**, 2025 (1998).
[15] X. Gan, S. Schilders, and M. Gu, Microsc. Microanal. **3**, 495 (1997).
[16] S. P. Schilders, X. S. Gan, and M. Gu, Appl. Opt. **37**, 5320 (1998).
[17] J. M. Schmitt, A. Knuttel, and M. Yadlowsky, J. Opt. Soc. Am. A **11**, 2226 (1994).
[18] Min Gu, T. Tannous, and C. R. J. Sheppard, Opt. Lett. **21**, 312 (1996).
[19] Yici Guo, Q. Z. Wang, N. Zhadin, F. Liu, S. Demos, D. Calistru, A. Tirksliunas, A. Katz, Y. Budansky, P. P. Ho, and R. R. Alfano, Appl. Opt. **36**, 968 (1997).
[20] S. P. Schilders and M. Gu, Appl. Opt. **38**, 720 (1999).
[21] C. Mar Blanca and C. Saloma, Appl. Opt. **37**, 8092 (1998).
[22] V. Daria, C. Mar Blanca, O. Nakamura, S. Kawata, and C. Saloma, Appl. Opt. **37**, 7960 (1998).
[23] X. Gan and M. Gu, Opt. Lett. **24**, 741 (1999).
[24] C. F. Bohern and D. R. Huffman, *Absorption and Scattering of Light by Small Particles* (Wiley, New York, 1983).
[25] V. E. Centonze and J. G. White, Biophys. J. **75**, 2015 (1998).
[26] D. Day and M. Gu, Appl. Opt. **37**, 6299 (1998).